ACS APPLIED MATERIALS & INTERFACES

RESEARCH ARTICLE

www.acsami.org

Ti-Doped Indium Tin Oxide Thin Films for Transparent Field-Effect Transistors: Control of Charge-Carrier Density and Crystalline Structure

Ji-In Kim,[†] Kwang Hwan Ji,[†] Mi Jang,[‡] Hoichang Yang,*[,‡] Rino Choi,[†] and Jae Kyeong Jeong*[,†]

[†]Department of Materials Science and Engineering and [‡]Department of Advanced Fiber Engineering, Inha University, Incheon 402-751, Korea

Supporting Information

ABSTRACT: Indium tin oxide (ITO) films are representative transparent conducting oxide media for organic light-emitting diodes, liquid crystal displays, and solar cell applications. Extending the utility of ITO films from passive electrodes to active channel layers in transparent field-effect transistors (FETs), however, has been largely limited because of the materials' high carrier density (>1 × 10^{20} cm^{-3}), wide band gap, and polycrystalline structure. Here, we demonstrate that control over the cation composition in ITO-based oxide films via solid doping of titanium (Ti) can optimize the carrier concentration and suppress film crystallization. On 120 nm thick SiO_2/Mo (200 nm)/glass substrates, transparent n-type FETs prepared with 4 at % Ti-doped ITO films and fabricated via the cosputtering of ITO and TiO_2 exhibited high electron mobilities of 13.4 cm^2 V^{-1} s^{-1}, a low subthreshold gate swing of 0.25 V $decade^{-1}$, and a high I_{on}/I_{off} ratio of >1 × 10^8.

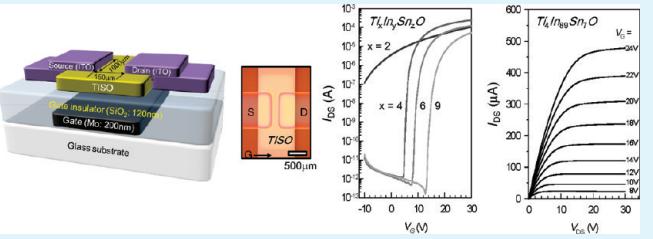

KEYWORDS: amorphous metal oxide, In−Sn−Ti-O, field-effect transistor, thin film transistor, transparent, oxygen vacancy

1. INTRODUCTION

Metal oxide-based field-effect transistors (FETs) have recently received considerable attention as strong candidates for realizing flexible, large-area, low-cost electronic devices, such as active matrix displays, electronic paper, and smart identification cards. These applications are enabled by their intriguing properties, including their high mobility, low-temperature processing, and reasonable reliability, in comparison to their counterpart amorphous Si FETs.[1] Among transistor device parameters, the field-effect mobility (μ_{FET}) is the most important. High charge-carrier transport requires a high driving current on a pixel FET and fast operational speeds in the associated integrated electronic circuits, such as the scan driver and data drive.[2]

Single metal oxide-based FETs containing either ZnO or In_2O_3 have achieved high μ_{FET} values.[3] However, when used as channel layers, these oxide films show polycrystalline phases with discernible distributions in the grain size and boundaries, depending on the film processing conditions. Control over the film uniformity plays an important role in achieving reliable μ_{FET} values and threshold voltages (V_{th}) in FETs for backplane electronics or integrated circuit applications. Complementary circuit designs can overcome nonuniformity issues to a certain extent, but such steps do not remove the barrier to producing high-yield and low-cost oxide FETs.[4] Amorphous metal oxides are anticipated to provide FETs with electrical performance properties that are better and more reliable than those of crystalline semiconductors.

Multicomponent oxides (MCOs) assume a variety of composition-dependent film structures that can be controlled by the addition of a network former, a mobility enhancer, and a carrier suppressor.[5] MCO films that include cation substitutional dopants (carrier generators) show high carrier densities of >1 × 10^{20} cm^{-3} and good transparencies toward visible light.[6] Among the various MCOs, the composition-dependent physical properties of transparent InSnO (ITO),[7] InZnO,[8] and ZnInSnO[9] have been intensively studied. The optical band gaps, subgap states, μ_{FET}, and net carrier densities have been characterized to evaluate their potential use as conducting oxide films. In addition, InGaZnO[10] and ZnInSnO films[11] have recently been investigated as promising semiconductor channel materials for FETs. Prior to their use in applications, the crystal-to-amorphous phase transition in MCO thin films must be systematically investigated.

Herein, we have investigated the phase transition behavior in Ti-assisted ITO (referred to herein as TiInSnO) films fabricated via cosputtering of ITO (In_2O_3 10 wt % SnO_2) and TiO_2 targets. In this case, SnO_2, In_2O_3, and titanium dioxide (TiO_2) were used, respectively, as the network former, mobility enhancer, and charge suppressor. TiO_2 is relatively inexpensive, and the electronegativity of Ti cations is comparable to the electronegativities of Hf,[12] Zr,[13] and Sc,[14] thus making it an attractive carrier suppressor for use in metal oxide semiconductors. Optical, structural, and electrical analyses of TiInSnO thin films with varying degrees of Ti loading levels have revealed that single-target

Received: March 30, 2011
Accepted: June 13, 2011
Published: June 13, 2011

dx.doi.org/10.1021/am200388h | ACS Appl. Mater. Interfaces 2011, 3, 2522–2528

sputtered ITO thin films with transparent polycrystalline electrodes can be tuned to form amorphous-like n-type semiconducting layers due to the dramatic suppression of the carrier density upon increasing the cosputtering power of the TiO_2 target. By optimizing the TiInSnO film structure, top-contact electrode FETs formed from 4 at % Ti-doped ITO films can be produced that show a high mobility of up to 13.4 $cm^2 V^{-1} s^{-1}$, a low subthreshold gate swing (SS) of 0.25 V $decade^{-1}$, and a high I_{on}/I_{off} ratio of $>1 \times 10^8$.

2. EXPERIMENTAL SECTION

2.1. Film Preparation. A 11−12 nm thick TiInSnO thin film was deposited on either a glass substrate, for evaluating the optical and structural properties, or on a SiO_2/Mo/glass substrate, to form an FET channel layer, by cosputtering dual ITO and TiO_2 targets. During the preparation of the semiconductor films, both targets were placed approximately 10 cm from the substrate. The working pressure was 0.26 Pa and the relative oxygen flow rate $[O_2]/[Ar+O_2]$ was maintained at 0.44. The DC power density of the ITO target was fixed at 2.2 W cm^{-2}, and the RF power density of TiO_2 was varied from 0 to 4.4 W cm^{-2}. A relatively thick TiInSnO film (50 nm) was used to measure the transmittance and absorbance, whereas the thickness of the active layer of a TiInSnO FETs was 11−12 nm.

2.2. Film Characterization. The surface morphology and roughness of the TiInSnO thin films were characterized by tapping-mode atomic force microscopy (AFM) using a Veeco Multimode IIIa. The optical properties of the TiInSnO films were analyzed using a Cary 5000 UV−vis-NIR spectrophotometer in the range 300−800 nm. Synchrotron-based two-dimensional (2D) grazing-incidence X-ray diffraction (GIXD) experiments on TiInSnO films with various Ti fractions were performed at the X9 beamline of the National Synchrotron Light Source (NSLS) at the Brookhaven National Laboratory. Each sample was mounted on a two-axis goniometer on top of an x-z stage, and the scattering intensity was recorded using a 2D Mar CCD detector. The structural properties of the TiInSnO films were double-checked by collecting a high-resolution X-ray diffraction scan (X PET-PRO MRD using Cu $K_{\alpha 1}$ source). The cation compositions and chemical state of the TiInSnO thin films were examined using X-ray fluorescence spectroscopy (XRF, Themoscientific, ARL Quant'X) and X-ray photoelectron spectroscopy (XPS), respectively.

2.2. FETs Fabrication and Characterization. Mo (200 nm) gate electrodes were deposited and patterned by conventional photolithography on a glass substrate. A 120 nm thick SiO_2 film was then grown on the substrate by plasma enhanced chemical vapor deposition for use as a gate dielectric. A 11−12 nm thick TiInSnO channel layer was prepared by cosputtering an ITO target and TiO_2 target. The active area was defined using a shadow mask during the deposition of the TiInSnO film, and the ITO source/drain (S/D) electrodes were deposited using the same sputtering system. The fabricated FETs had a bottom gate structure, and their channel widths (W) and lengths (L) were 1000 and 150 μm, respectively. The devices were annealed in air for 1 h at 240 °C. The transfer characteristics of the TiInSnO FETs were measured using a Keithley 2636 Source Meter at room temperature.

3. RESULTS AND DISCUSSION

TiInSnO films containing different Ti fractions were fabricated by cosputtering with dual ITO and TiO_2 targets (see the Experimental Section). Note that cosputtering was performed with a fixed ITO target power of DC 100 W and a selected RF power of 0−200 W (for the TiO_2 target). The as-deposited TiInSnO films were then thermally annealed in ambient air for 1 h at 240 °C. Table 1 summarizes the compositional variations

Table 1. In, Sn, and Ti Content of the TiInSnO Films As a Function of the TiO_2 RF Power, under a Fixed ITO DC power of 100 W[a]

		cation composition (at %)		
samples	TiO_2 rf power (W)	In	Sn	Ti
ITO		92.4	7.6	
$Ti_2In_{91}Sn_7O$	60	90.8	7.2	2.0
$Ti_4In_{89}Sn_7O$	100	89.0	7.4	3.6
$Ti_6In_{88}Sn_6O$	150	88.1	5.9	6.0
$Ti_9In_{88}Sn_4O$	200	87.7	3.4	8.9

[a] The atomic ratio of the TiInSnO film was analyzed by XRF. The ratio of Ti/(In+Sn+Ti) increased monotonically with increasing TiO_2 DC power.

in the 11−12 nm thick TiInSnO films on the SiO_2/Si substrates as a function of the RF power of the TiO_2 target, based on the XRF cation analysis. In the TiInSnO films, the Ti^{4+} and Sn^{4+} contents increased monotonically from 0 to 9 at.% and decreased from 7.6 to 3.4 at %, respectively, as the RF power applied to the TiO_2 target was increased from 0 to 200 W. In contrast, the In content changed slightly from 92 to 88 at % over the same increase in RF power. Figure 1a shows the AFM topography of the ITO film (top) and $Ti_4In_{89}Sn_7O$ film (bottom), which revealed that the TiInSnO films had homogeneous smooth textures without local aggregation, and they had a small root-mean square surface roughness of 0.1−0.2 nm (2 μm × 2 μm) that was comparable to that of the ITO film (also see Figure S1 in the Supporting Information). The results suggested that during the cosputtering process, Sn^{4+} ions located at the sublattice sites of In_2O_3 crystals were preferentially substituted with Ti^{4+} ions. The incorporated Ti^{4+} ions (with a smaller radius than Sn^{4+})[15] were expected to significantly affect the degree of compositional and configurational order in the system. Below, we discuss the effects of incorporating Ti into TiInSnO films on the crystalline structure, as investigated through X-ray analysis.

The role of Ti additives on the optical properties of the $Ti_xIn_ySn_zO$ film system (x = 2, 4, 6, 9) was investigated by fabricating ITO and TiInSnO films on glass substrates. Figure 1b shows the optical transmission spectra of 50 nm thick ITO and $Ti_xIn_ySn_zO$ films prepared with various metal compositions. Note that the film thicknesses were much greater than those (11−12 nm) of the samples used in the FETs. Thicker films yielded amplified variations in the optical properties of Ti-assisted ITO films as a function of the Ti content (at %). All TiInSnO films were optically transparent and colorless and were less dependent on the Ti content: they showed an average transmittance (T_{ave}) exceeding 70% in the visible region, which was comparable to that of the glass substrate, that is, T_{ave} > 80%. In contrast, the optical band gap (E_g^{opt}) differed noticeably between the ITO-only and TiInSnO films. The values of E_g^{opt} were determined by extrapolating the best fit line in the plot of $(\alpha h\nu)^2$ versus $h\nu$ to the intercept (at α = 0) for the ITO and $Ti_xIn_ySn_zO$ (x = 4, 6, 9) systems (see Figure 1c).[16] As the Ti at % in the TiInSnO films increased, the E_g^{opt} values increased dramatically from 3.60 eV (for ITO) to 3.96 eV (for $Ti_9In_{88}Sn_3O$). Variations in E_g^{opt} arose mainly from the Ti-assisted structural changes from the crystalline to the amorphous phases.

The incorporation of Ti significantly affected the interactions between the nearest neighbor components, as determined by

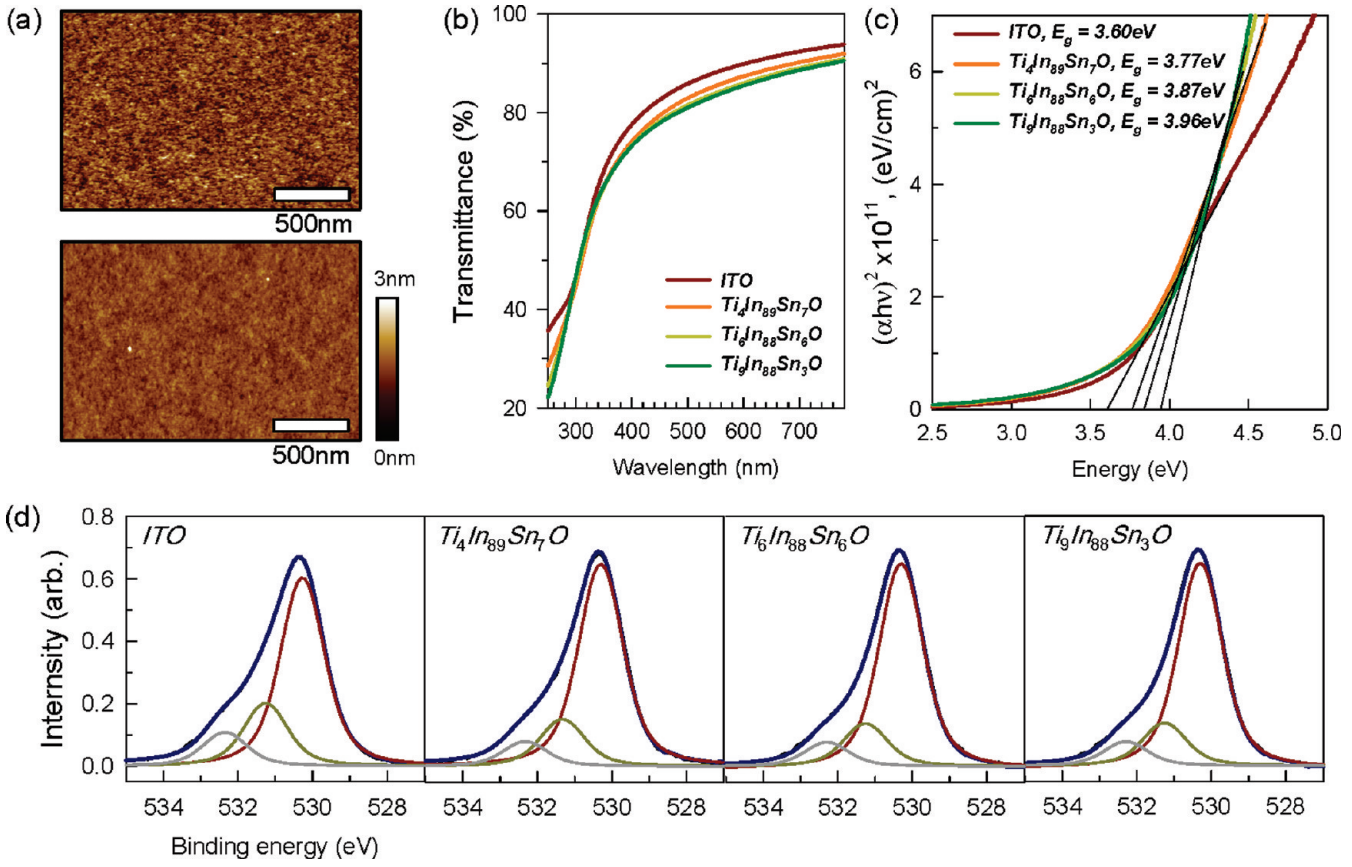

Figure 1. (a) Tapping-mode AFM images of ITO (top) and TiInSnO (bottom) films prepared under vacuum conditions at a TiO_2 RF power of 100 W. (b) Optical transmittance of ITO and TiInSnO films, and (c) plot of $(\alpha h\nu)^2$ versus hν for calculation of the optical band gap for each thin film. (d) O1s XPS spectra of the TiInSnO films with different Ti contents.

XPS. Figure 1d shows the O1s XPS spectra of TiInSnO films with different Ti contents. The O1s peaks centered at binding energies of 530.1 or 531.0 eV arose from the oxygen atoms in, respectively, the oxide lattices without or with oxygen vacancies (summarized in Table S1 in the Supporting Information).[17] The peak areas of the oxygen vacancies clearly decreased as the Ti fraction increased. A larger portion of reduced oxygen vacancies in the higher Ti content films suggested that the free carrier density decreased, which enabled the resulting TiInSnO films to act as efficient channel materials. In the context of In_2O_3-based oxide semiconductors, the electrical role of oxygen vacancies [V_O] has inspired debate. Kamiya et al. reported that the V_O states in the In−Ga−Zn−O system are deep levels, as determined by ab initio calculations.[18] On the other hand, Agoston et al. reported that the V_O states in the In_2O_3 system are shallow states capable of creating free electrons in the conduction band, using the same first-principle calculations.[19] A similar metastable shallow state for V_O was also predicted for ZnO and In_2O_3.[20] Existing V_O models for In_2O_3 and its derivative materials were inconclusive with regards to the calculated electronic structures. Experimental observations strongly indicated that V_O defects provided a source of n-type conductivity (>1 × 10^{20} cm^{-3}).[21] Moreover, strong correlations between the oxygen vacancy level and the n-type carrier density has been reported for In−Ga−Zn−O,[22] Ga−Zn−Sn−O,[23] and Zr−Zn−Sn−O[24] films. In these reports, reductions in the free electron density were strongly associated with fewer oxygen vacancy defects. Therefore, in this study, it would be reasonable to assume that lower V_O concentrations and higher TiO_2 fractions would reduce the free electron density, permitting the resulting oxide TFTs on/off current ratio to be modulated, as shown below.

The ITO and TiInSnO films prepared on SiO_2/Si substrates via sputtering and annealing were analyzed using several X-ray techniques. As shown in Figure 2, the X-ray reflectivities of these films indicated that the sputtered films had smooth uniform surfaces. The inset of Figure 2 shows that the oscillation period of the X-ray reflectivity in reciprocal space was given by $\Delta q_z = 2\pi/t_s$, where t_s is the thickness of the active layer. The value of Δq_z permitted the accurate determination of the thickness of the ITO and Ti−In−Sn-O films to 11−12 nm (details are provided in the Supporting Information). Figure 3a shows the 2D GIXD patterns of the 11−12 nm thick ITO and $Ti_xIn_ySn_zO$ films. Because of the high In fraction (approximately 92 at %) in the ITO film, the GIXD pattern for the ITO-only system clearly showed a typical powderlike ring pattern corresponding to the polycrystalline In_2O_3 with a bixbyite structure (C-type rare-earth crystal structure) at q = 1.546, 2.194, 2.508, 2.979, 3.243, and 3.604 $Å^{-1}$, corresponding to the (211), (222), (400), (332), (431), and (440) planes, respectively.[25] These results strongly supported the assertion that polycrystalline In_2O_3 acted as a network former with a body-centered cubic phase (*Ia*3, number 206) characterized by a lattice parameter of 10.03 Å.[25] In particular, the Debye ring pattern of the ITO film revealed that the In_2O_3 crystallites

were randomly distributed without any preferential orientations. The average grain size (D) of the ITO crystallites was estimated to be 4.5 ± 0.5 nm using Scherrer's equation ($D = k\lambda/\beta\cos\theta$, where k is a constant assumed to be 0.98, λ is the wavelength of the incident X-rays, β is the full width at half-maximum intensity of the (222) diffraction peak, and θ is the diffraction angle at $q_{(222)}$).[26]

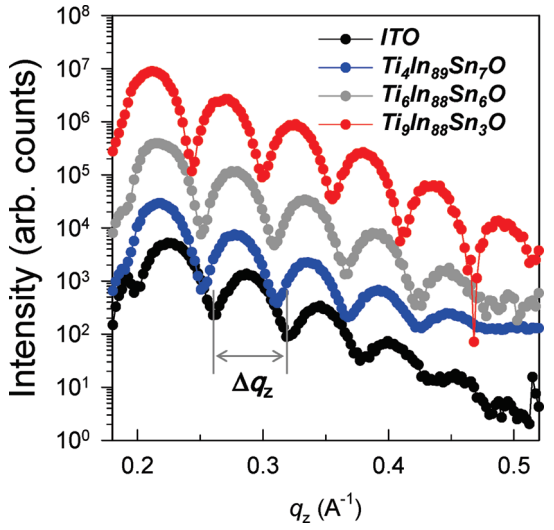

Figure 2. X-ray reflectivity profiles of ITO and $Ti_xIn_ySn_zO$ films with different Ti contents. The film thicknesses (t_s, see Table S2 in the Supporting Information) was calculated by the following equation: $\Delta q_z = 2\pi/t_s$, where Δq_z is the periodic distance between the X-ray reflectivity peak-to-peak.

The 2D GIXD patterns of the TiInSnO films (see Figure 3a) clearly showed that the peak intensities of In_2O_3, specifically those from the (222) crystal planes, decreased dramatically as the Ti at % increased. As shown in Figure 3b, a higher volume of the 4 at % Ti-incorporated ITO film was amorphous rather than crystalline, as indicated by the broad X-ray peak. Films exceeding 9 at % Ti ($Ti_9In_{88}Sn_3O$) provided no evidence for In_2O_3 crystallites in the GIXD patterns. Only an amorphous hollow peak remained, indicating that Ti was incorporated into the sputtered MCO films and induced a phase transition from a crystalline to an amorphous solid. Short-range atomic ordering was disrupted because Ti^{4+} ions were smaller Sn^{4+}. The Ti-assisted phase was thermodynamically stable and did not recover to the crystalline form, even after thermal annealing at 240 °C for several hours. Because no peaks were observed in the GIXD patterns of these annealed films, the TiInSnO films contained homogeneous nanostructures in which the Ti-dependent crystallinity was controllable without the use of metallic segregation techniques. The optical and structural results suggested that the Ti-assisted ITO film may provide a promising transparent channel material for use in large-area electronic applications.

The electrical characteristics of the TiInSnO-based FETs depended on the amount of Ti incorporated, as characterized by measurements of 11−12 nm thick TiInSnO films (Figure 4a) selectively patterned onto SiO_2 (120 nm)/Mo/glass substrates through a mask via cosputtering in a chamber. The samples were postannealed at 240 °C for 1 h, and top-contact ITO electrodes were sputtered onto the MCO films (see the Experimental Section). Figure 4b presents a schematic diagram illustrating the resulting TiInSnO-based FETs. As expected from the UV−vis spectra (Figure 1b), the typical optical microscopy images of the resulting devices showed FETs with an optically

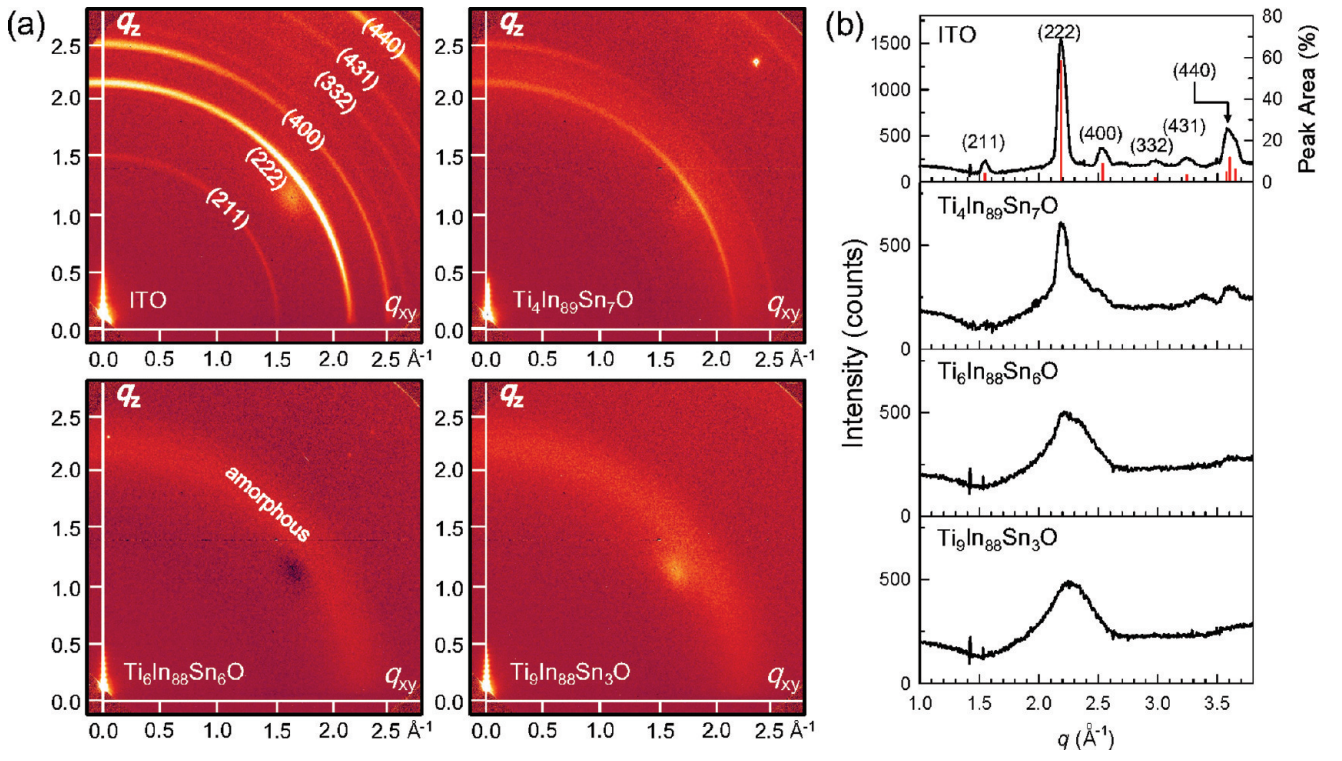

Figure 3. (a) Two-dimensional GIXD patterns of 11−12 nm thick ITO and $Ti_xIn_ySn_zO$ films. (b) Out-of-plane GIXD patterns of the TiInSnO films with different Ti contents.

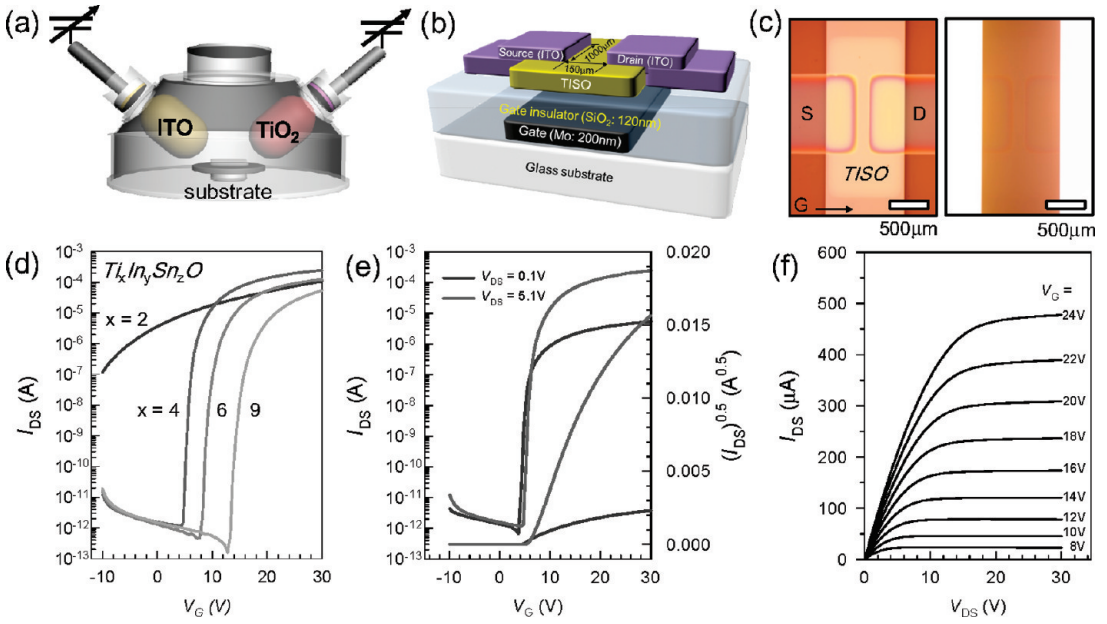

Figure 4. (a) Schematic illustration of a cosputtering apparatus used for the preparation of TiInSnO films. (b) Three-dimensional schematic diagram of the TiInSnO FETs with an inverted staggered bottom gate structure. (c) Typical optical microscopy images of the resulting devices showing FETs with an optically transparent structure. Left side (reflection mode) and right side (transmission mode). (d) Variations in the transfer characteristics of $Ti_xIn_ySn_zO$-based FETs as a function of the incorporated Ti content. The representative (e) transfer and (f) output characteristics of the TiInSnO-based FETs, including $Ti_4In_{89}Sn_7O$ thin film.

Table 2. Electrical Characteristics of FETs Based on $Ti_xIn_ySn_zO$ Films with Different Ti Contents

samples	μ_{FET} ($cm^2\ V^{-1}\ s^{-1}$)	SS (V $decade^{-1}$)	V_{th} (V)	I_{on}/I_{off}	D_{it} ($eV^{-1}\ cm^{-2}$)	N_{ss} ($eV^{-1}\ cm^{-3}$)
$Ti_2In_{91}Sn_7O$		2.47	−14.33	1.0×10^3	7.3×10^{12}	5.0×10^{18}
$Ti_4In_{89}Sn_7O$	13.4	0.25	5.30	1.0×10^8	5.8×10^{11}	5.0×10^{17}
$Ti_6In_{88}Sn_6O$	8.8	0.42	9.07	9.7×10^7	1.1×10^{12}	8.5×10^{17}
$Ti_9In_{88}Sn_4O$	6.2	0.59	14.46	3.7×10^7	1.6×10^{12}	1.2×10^{18}

transparent structure, even though a relatively thick patterned Mo electrode (200 nm) was used as the gate metal on the glass substrate (see Figure 4c).

Figure 4d shows the variations in the transfer characteristics of the $Ti_xIn_ySn_zO$-based FETs as a function of the incorporated Ti content. The ITO-only FET exhibited a simple conducting behavior. The on/off current ratio (I_{on}/I_{off}) was not modulated. This property was attributed to a high net carrier density of 1.05×10^{20} cm^{-3} resulting from the polycrystalline nature of the material (see Figure 3a), calculated from the Hall effect measurement. Unlike the ITO-based FET, the incorporation of Ti into the ITO films resulted in moderate transistor behavior. Incorporation of Ti produced a clear pinch-off. A saturated I_{DS} was observed, as shown in Figure 4d, indicating that electron transport in the TiInSnO active channel was controlled by the gate and drain voltages. The absence of creep in the I_{DS} in the low V_{DS} voltage region indicated the presence of Ohmic contact between the ITO source/drain electrodes and TiInSnO. The important device parameters of the $Ti_xIn_ySn_zO$ FETs as a function of the Ti fraction are summarized in Table 2. The μ_{FET} was determined by the maximum trans-conductance at a drain voltage (V_{DS}) of 0.1 V, and V_{th} was determined by the gate voltage (V_{GS}) required to produce a drain current of $L/W \times 10$ nA at V_{DS} = 5.1 V (see Figure 4e). The subthreshold gate swing ($SS = dV_{GS}/d\log I_{DS}$) was extracted from the linear portion of a plot of the $\log I_{DS}$ versus V_G.

For the TiInSnO-based FETs, device performances were optimized for the $Ti_4In_{89}Sn_7O$ thin film: μ_{FET}, SS, V_{th}, and I_{on}/I_{off} were, respectively, 13.4 $cm^2\ V^{-1}\ s^{-1}$, 0.25 V $decade^{-1}$, 5.3 V, and $>1 \times 10^8$. Above $x = 4$, the $Ti_xIn_ySn_zO$ thin films become more resistive, indicating that V_{th} in the corresponding FETs were shifted toward positive values. In this case, the values of μ_{FET} and V_{th} were reduced to 6.2 $cm^2\ V^{-1}\ s^{-1}$ and 14.5 V for the $Ti_9In_{88}Sn_3O$ FET, although the value of I_{on}/I_{off} was comparable to that of the optimized $Ti_4In_{89}Sn_7O$ FET.

The *SS* value of a given FET device is related to the total density of traps, including the bulk (N_{SS}) and semiconductor−insulator interfacial traps (D_{it}), according to[27]

$$SS = \frac{qk_BT(N_{SS}t_{ch} + D_{it})}{C_i log(e)} \quad (1)$$

where q is the electron charge, k_B is Boltzmann's constant, T is the absolute temperature, and t_{ch} is the channel layer thickness.

N_{SS} and D_{it} in the Ti-based ITO FET were calculated by setting one of parameters equal to zero. In the present study, the values of N_{SS} and D_{it} correspond to the maximum trap density formed in a given system. For example, the values of N_{SS} and D_{it} for the $Ti_4In_{89}Sn_7O$-based FET were 5.04×10^{17} $eV^{-1}\ cm^{-3}$ and 5.76×10^{11} $eV^{-1}\ cm^{-2}$, respectively, which were comparable to those (N_{SS}, $1-6 \times 10^{17}$ $eV^{-1}\ cm^{-3}$; D_{it}, $4-8 \times 10^{11}$

eV^{-1} cm^{-3}) of the InGaZnO[28] and ZnInSnO[29] FETs. For other FETs with different Ti contents, however, these values increased dramatically with increasing Ti content (see Table 2). For the $Ti_9In_{88}Sn_3O$ FET, the N_{SS} and D_{it} values were 1.19×10^{18} eV^{-1} cm^{-3} and 1.60×10^{12} eV^{-1} cm^{-2}, respectively. This strongly supported the conclusion that the addition of excess Ti cations broadened the gap state of the TiInSnO semiconductor.

Taken together, these results indicate that the appropriate amount of Ti cations should be carefully incorporated to achieve control over the carrier density (1×10^{17} cm^{-3}) and amorphous phase state of a multicomponent oxide semiconductor without creating a significant gap state. Thus, in this study, the recommended Ti cation fraction for the ITO-based channel system was determined to be 4.0 at %, although this value depends on the channel materials, process temperature, film preparation method, and device configuration.

4. CONCLUSION

We clarified the role of TiO_2 incorporation into ITO films. GIXD and XPS measurements demonstrated that the addition of Ti to a ITO lattice hindered the conversion of the film into a crystalline phase and, simultaneously, efficiently suppressed creation of a high carrier concentration via formation of oxygen vacancies during heat treatment of the as-deposited TiInSnO film. An amorphous TiInSnO film containing an optimum Ti fraction provides a promising semiconductor material: FETs with the optimum Ti composition of 4.0 at % exhibited a high mobility of 13.4 cm^2 V^{-1} s^{-1}, low subthreshold gate swing of 0.25 V $decade^{-1}$, and a high I_{on}/I_{off} ratio of $>1 \times 10^8$. However, when the Ti fraction exceeded 6.0 at.%, the fabricated FETs suffered from reduced mobility and high V_{th} values (>9 V), suggesting that the excessive incorporated TiO_2 strongly suppressed the carrier concentration, causing the resulting TiInSnO thin film to exhibit insulating properties.

■ ASSOCIATED CONTENT

Supporting Information. AFM images of vacuum-derived ITO and TiInSnO films and the deconvolution data of XPS O1s peaks. This material is available free of charge via the Internet at http://pubs.acs.org/.

■ AUTHOR INFORMATION

Corresponding Author

*E-mail: hcyang@inha.ac.kr (H.Y.); jkjeong@inha.ac.kr (J.K.J.).

■ ACKNOWLEDGMENT

This work was supported by the Basic Science Research Program through the National Research Foundation of Korea (NRF) funded by the Ministry of Education, Science and Technology (2010-0028223 and 2010-0008982) and the Converging Research Center Program through the Ministry of Education, Science and Technology (2010K001062). It was also partly supported by the IT R&D Program of MKE/KEIT (KI002182).

■ REFERENCES

(1) Nomura, K.; Ohta, H.; Takagi, A.; Kamiya, T.; Hirano, M.; Hosono, H. *Nature* **2004**, *432*, 488.

(2) Wager, J. F.; Keszler, D. A.; Presley, R. E. In *Transparent Electronics*, 1st ed.; Springer: New York, 2007; Chapter 6.

(3) (a) Fortunato, E.; Barquinha, P.; Pimentel, A.; Goncalves, A.; Marques, A.; Pereira, L.; Martins, R. *Adv. Mater.* **2005**, *17*, 590–594. (b) Wang, L.; Yoon, M.-H.; Lu, G.; Yang, Y.; Facchetti, A.; Marks, T. J. *Nat. Mater.* **2006**, *5*, 893–900.

(4) (a) Lin, C.-L.; Chen, Y.-C. *IEEE Electron Device Lett.* **2007**, *28*, 129–131. (b) Jung, S. H.; Nam, W. J.; Han, M. K. *IEEE Electron Device Lett.* **2004**, *25*, 690–692.

(5) Hosono, H. *J. Non-Cryst. Solids* **2006**, *352*, 851–858.

(6) Hoel, C. A.; Mason, T. O.; Gaillard, J.-F.; Poeppelmeier, K. R. *Chem. Mater.* **2010**, *22*, 3569–3579.

(7) (a) Kim, H.; Gilmore, C. M.; Pique, A.; Horwitz, J. S; Murata, H.; Kafafi, Z. H.; Chrisey, D. B. *J. Appl. Phys.* **1999**, *86*, 6451–6461. (b) Mizuhashi, M. *Thin Solid Films* **1980**, *70*, 91–100. (c) Ohta, H.; Orita, M.; Hirano, M.; Tanji, H.; Kawazoe, H.; Hosono, H. *Appl. Phys. Lett.* **2000**, *76*, 2740–2742.

(8) (a) Naghavi, N.; Marcel, C.; Dupont, L.; Rougier, A.; Leriche, J.-B.; Guery, C. *J. Mater. Chem.* **2000**, *10*, 2315–2319. (b) Phillips, J. M.; Cava, R. J.; Thomas, G. A.; Carter, S. A.; Kwo, J.; Siegrist, T.; Krajewski, J. J.; Marshall, J. H.; Peck, W. F.; Rapkine, D. H. *Appl. Phys. Lett.* **1995**, *67*, 2246–2248.

(9) (a) Minami, T.; Kakumu, T.; Shimokawa, K.; Takata, S. *Thin Solid Films* **1998**, *317*, 318–321. (b) Liu, D.-S.; Lin, C.-H.; Huang, B.-W.; Wu, C.-C. *Jpn J. Appl. Phys.* **2006**, *45*, 3526–3530.

(10) (a) Yabuta, H.; Sano, H.; Abe, K.; Aiba, T.; Den, T.; Kumomi, H.; Nomura, K.; Kamiya, T.; Hosono, H. *Appl. Phys. Lett.* **2006**, *89*, 112123. (b) Jeong, J. K.; Jeong, J. H.; Yang, H. W.; Park, J.-S.; Mo, Y.-G.; Kim, H. D. *Appl. Phys. Lett.* **2007**, *91*, 113505.

(11) Ryu, M. K.; Yang, S.; Park, S.-H. K.; Hwang, C.-S.; Jeong, J. K. *Appl. Phys. Lett.* **2009**, *95*, 173508.

(12) Kim, C.-J.; Kim, S.; Lee, J.-H.; Park, J.-S.; Kim, S.; Park, J.; Lee, E.; Lee, J.; Park, Y.; Kim, J. H.; Shin, S. T.; Chung, U.-I. *Appl. Phys. Lett.* **2009**, *95*, 252103.

(13) Park, J.-S.; Kim, K. S.; Park, Y.-G.; Mo, Y.-G.; Kim, H. D.; Jeong, J. K. *Adv. Mater.* **2009**, *21*, 329–333.

(14) Choi, Y.; Kim, G. H.; Jeong, W. H.; Bae, J. H.; Kim, H. J.; Hong, J.-M.; Yu, J.-W. *Appl. Phys. Lett.* **2010**, *97*, 162102.

(15) Oxtoby, D. W.; Nachtrieb, N. H. In *Principles of Modern Chemistry*, 2nd ed.; Saunders College Publishing: Philadelphia, PA, 1990; Appendix F.

(16) Tauc, J. *Mater. Res. Bull.* **1968**, *3*, 37–46.

(17) (a) Fan, J. C. C.; Goodenough, J. B. *J. Appl. Phys.* **1997**, *48*, 3524–3531. (b) Ishida, T.; Kobayashi, H.; Nakato, Y. *J. Appl. Phys.* **1993**, *73*, 4344–4350. (c) Major, S.; Kumar, S.; Bhatnagar, M.; Chopra, K. L. *Appl. Phys. Lett.* **1986**, *49*, 394–396.

(18) Kamiya, T.; K. Nomura, K.; Hosono, H. *Sci. Technol. Adv. Mater.* **2010**, *11*, 044305.

(19) Agoston, P.; Erhart, P.; Klein, A.; Albe, K. *J. Phys.: Condens. Matter* **2009**, *21*, 455801.

(20) Lany, S.; Zunger, A. *Phys. Rev. Lett.* **2007**, *98*, 045501.

(21) (a) Shigesato, Y.; Takaki, S.; Haranoh, T. *J. Appl. Phys.* **1992**, *71*, 3356–3364. (b) Ito, N.; Sato, Y.; Song, P. K.; Kaijio, A.; Inoue, K.; Shigesato, Y. *Thin Solid Films* **2006**, *496*, 99–103. (c) Yaglioglu, B.; Huang, Y.-J.; Yeom, H.-Y.; Paine, D. C. *Thin Solid Films* **2006**, *496*, 89–94. (d) Jung, Y. S.; Seo, J. Y.; Lee, D. W.; Jeon, D. Y. *Thin Solid Films* **2003**, *445*, 63–71. (e) Bhosle, V.; Tiwari, A.; Narayan, J. *Appl. Phys. Lett.* **2006**, *88*, 032106.

(22) (a) Jeong, S.; Ha, Y.-G.; Moon, J.; Facchetti, A.; Marks, T. J. *Adv. Mater.* **2010**, *22*, 1346. (b) Bae, C.; Kim, D.; Moon, S.; Choi, T.; Kim, Y.; Kim, B. S.; Lee, J.-S.; Shin, H.; Moon, J. *ACS Appl. Mater. Interfaces* **2010**, *2*, 626–632.

(23) Jeong, Y.; Bae, C.; Kim, D.; Song, K.; Woo, K.; Shin, H.; Cao, G.; Moon, J. *ACS Appl. Mater. Interfaces* **2010**, *2*, 611–615.

(24) Rim, Y. S.; Kim, D. L.; Jeong, W. H.; Kim, H. J. *Appl. Phys. Lett.* **2010**, *97*, 233502.

(25) Marezio, M. *Acta Crystallogr.* **1966**, *20*, 723–728.

(26) Azaroff, L. V. *Elements of X-ray Crystallography*; McGraw-Hill Book Company: New York, 1968; p 552.

(27) Greve, D. W. *Field Effect Devices and Application: Devices for Portable Low Power and Imaging Systems*, 1st ed.; Prentice-Hall: Englewood Cliffs, NJ, 1998.
(28) Jeong, J. K.; Jeong, J. H.; Yang, H. W.; Park, J.-S.; Mo, Y.-G.; Kim, H. D. *Appl. Phys. Lett.* **2007**, *91*, 113505.
(29) Ryu, M. K.; Yang, S.; Park, S.-H. K.; Hwang, C.-S.; Jeong, J. K. *Appl. Phys. Lett.* **2009**, *95*, 072104.